J Mater Sci: Mater Med (2007) 18:2123–2129
DOI 10.1007/s10856-007-3012-y

Oxidized nickel–titanium foams for bone reconstructions: chemical and mechanical characterization

Maite Barrabés · Alexandra Michiardi · Conrado Aparicio · Pablo Sevilla · Josep A. Planell · Francisco Javier Gil

Received: 31 March 2006 / Accepted: 22 March 2007 / Published online: 10 July 2007

Abstract This work examines NiTi foams that have been treated using a new oxidation treatment for obtaining Ni-free surfaces that could allow the ingrowth of living tissue, thereby increasing the mechanical anchorage of implants. A significant increase in the real surface area of these materials can decrease corrosion resistance and favour the release of Ni. This chemical degradation can induce allergic reactions or toxicity in the surrounding tissues. This study determines the porosity, surface characteristics, phase transformation, mechanical properties, corrosion behaviour and Ni release into the simulated body fluid medium of foams treated by a new surface oxidation treatment that produces Ni-free surfaces. These foams have pores in an appropriate range of sizes and interconnectivity, and thus their morphology is similar to that of bone. Their mechanical properties are biomechanically compatible with bone. The titanium oxide on the surface significantly improves corrosion resistance and decreases nickel ion release, while barely affecting transformation temperatures.

Introduction

NiTi shape-memory alloys can be used in a wide range of biomedical applications. However, despite their unique and attractive shape-memory properties, superelasticity and excellent damping characteristics, they are still controversial because of the potentially toxic, allergic and carcinogenic effects of releasing Ni into the exterior medium [1–4].

To prevent adverse reactions to implants, researchers have studied surface treatments using a variety of approaches. The oxidation of NiTi material has been used to obtain surfaces with a low Ni content. This work focuses on surface oxidation treatments. NiTi alloys are highly biocompatible due to an inert protective TiO_2 layer that forms on the surface of the material [5]. However, depending on the thickness, composition and morphology of the layer, corrosion and ion release may vary [6]. In this work, we studied the oxidation treatment in a low oxygen pressure atmosphere, which provides a high surface Ti/Ni ratio, a very low Ni surface concentration and a thick oxide layer.

Several classes of synthetic osteoconductive and osteoinductive biomaterials have been researched, developed and marketed. In orthopaedics, these synthetic and naturally derived biomaterials are used to fill empty space in bone, to bridge and fill localized defects and to facilitate bone ingrowth. Many bioresorbable polymers, ceramics and ceramic pastes have little or no initial porosity, while cancellous bone graft and porous ceramics have relatively high porosity (35–60%).

Interconnected porosity is very important because bone grows in interconnected pore channels near the surface in a way that maintains vascularity and long-term viability and provides firm fixation. Optimal pore size has been found to be in the range of 100–400 μm [7, 8]. This open porous structure allows bone tissue to grow into the body of the implant, which provides firm fixation. Porosity also affects the mechanical behaviour of the material [9–11]. A good

M. Barrabés · A. Michiardi · C. Aparicio (✉) · P. Sevilla · J. A. Planell · F. J. Gil
CREB, Departamento de Ciencia de los Materiales e Ingeniería Metalúrgica, ETSEIB, Universidad Politécnica de Cataluña, Diagonal 647, 08028 Barcelona, Spain
e-mail: conrado.aparicio@upc.edu

match is required between the elastic modulus of the bone (20 GPa) and that of the implant. NiTi alloys in the martensitic phase have shown the closest values (28–41 GPa). Moreover, if the material has an internal structure with a porosity of 50%, it exhibits a lower modulus (14–20 GPa). Significant bone ingrowth is possible at this matching value.

In this work, we examine a new oxidation treatment that obtains NiTi foams with Ni-free surfaces. We determine Ni surface concentration, oxide thickness and oxide chemical composition using X-ray photoelectron spectroscopy (XPS). We study the transformation temperatures, mechanical properties, corrosion behaviour and ion release of treated and untreated alloys.

Materials and methods

Sample preparation

The cylinders of porous NiTi studied (NiTipore®) were produced by self-propagating high-temperature synthesis (SHS). This method, also known as ignition synthesis, applies the exothermic heat of formation to the interaction of nickel (Ni) and titanium (Ti). The temperature increase throughout the volume of the reacting system leads to a self-ignition similar to an explosion. In the reacting zones, the maximum temperature values can be lower than, equal to or slightly higher than the melting point of NiTi. This method allows good control of the porosity range. Thus, it provides appropriately sized and interconnected pores and creates morphology close to that of bone. Figure 1 shows the cylinders obtained.

Ten porous NiTi cylinders were sectioned using a diamond disc according to the requirements of each proposed test. All samples were lightly polished with 600-grit Al_2O_3 paper to remove contaminants from casting. The samples were then treated in order to form a Ni-depleted surface layer.

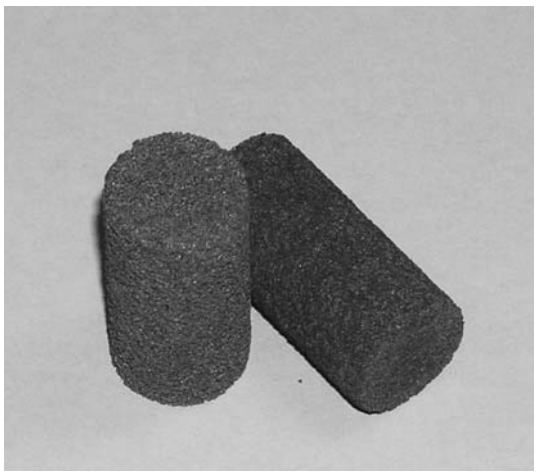

Fig. 1 Porous NiTi cylinders

The cylinders were homogenized in a tubular furnace (ST16, Hobersal, Spain) in an argon atmosphere at 1,100 °C for 6 h, with a heating ramp of 6 °C/min. They were then subjected to a thermal treatment in order to stabilize the β phase and activate the shape-memory properties. This treatment consisted of a 10-min heating phase at 800 °C, a cold-water quench, and a 1-h annealing at 500 °C. In order to produce the titanium oxide coating, the cylinders were thermally treated for 2 h and 30 min at a pressure of 3×10^{-2} mbar and a temperature of 400 °C [12, 13].

Pore size and distribution

A metallographic examination was carried out on various sections of five of the cylinders using optical (GX51, Olympus, Japan) and scanning electron microscopes (JSM 6400, Jeol, Japan) equipped with an image-analysis system (OmniMet, Buehler, USA). The samples were also studied by means of mercury pycnometry. Based on these observations, we determined the pore size, total porosity and isotropy.

Surface chemical composition

The surface chemical composition of the samples after treatment was determined by means of XPS (PHI5500, Physical Electronics, USA). The Ni concentration profile of the samples was determined by means of argon sputtering.

The surface of the samples was analysed by means of XPS. The XPS experiments were performed in a PHI 5500 Multitechnique System (Physical Electronics) with a monochromatic X-ray source (Aluminium Kα line with 1486.6 eV and 350 W), placed perpendicular to the analyser axis (takeoff angle: 45°) and calibrated using the 3d5/2 line of Ag with a full width at half maximum (FWHM) of 0.8 eV. The analysed area was a circle with a diameter of 0.8 mm. The selected resolution for the fitted spectra was 23.5 eV of pass energy and 0.1 eV/step. In-depth measurements and chemical composition depth profiles were obtained by sputtering the surface with an Ar^+ ion source (4 keV energy).

In these conditions, a 6 nm/min sputtering rate was determined as calibrated against a TiO_2 standard. These measurements were taken in an ultra-high vacuum chamber.

Multiplex (narrow-scan) spectra were obtained for C1s, O1s, $Ti2p_{3/2}$, $Ti2p_{1/2}$, $Ni2p_{3/2}$, $Ni2p_{1/2}$ and Ar1s photopeaks.

The obtained spectra were analysed using Multipak software (Physical Electronics, USA). All binding energies were referenced to the C1s peak at 284.8 eV, corresponding to adsorbed hydrocarbon (C-H) contamination at the surface. The atomic sensitivity factors included in the instrument data system were used to calculate the atomic concentration of the elements. The curve-fitting analysis was performed using a Gaussian-Lorentzian fitting. The oxide thickness was estimated based on the depth at which the oxygen signal had decreased to 50% of its maximum value [5, 14, 15]. One, two or three samples were analysed per group, depending on the surface treatment.

Phase-transformation temperatures

The effect of the oxidation treatment on the phase-transformation temperatures was also studied. The transformation temperatures were determined by means of differential scanning calorimetry (2920 Modulated DSC, TA Instruments, USA) with a heating ramp of 10 °C/min and a cooling ramp of 2 °C/min. M_s (martensite start) and M_f (martensite finish) are, respectively, the starting and finishing temperatures of martensite formation upon cooling from the austenite phase. Similarly, A_s (austenite start) and A_f (austenite finish) are, respectively, the starting and finishing temperatures of austenite formation upon heating from the martensitic phase.

The calibration was carried out with Indium and did not vary with the heating rate. After optimization in preliminary tests, a lower rate was used upon cooling to ensure a flat baseline and ensure accurate calculation of transformation temperatures and enthalpies (performed using appropriate software).

Compression tests

Compression tests were performed according to the ASTM 451 standard. Five specimens were tested in compression at a cross-head speed of 10 mm/min. The samples tested were cylindrical, with a diameter of 10 mm and a length of 30 mm. Load versus deflection was continuously monitored and recorded. These mechanical tests were performed using a MTS-Bionix 858 (MTS, USA) servo-hydraulic testing machine. The tests were performed at 37 °C.

Corrosion behaviour

The corrosion behaviour of the treated and untreated samples was studied by means of electrochemical techniques using a potentiostat (Voltalab PGZ 301, Radiometer, Denmark). The samples were connected as working electrodes, and Ag/AgCl and Pt electrodes were used as reference and counter electrodes, respectively. Hanks' balanced salt solution was used as electrolyte at 37 °C in order to simulate the physiological conditions.

Free potential and cyclic potential tests were carried out. In the former, the changes in the potential between the sample and the reference electrode were measured over time. In the latter, the potential between the sample and the reference electrode was progressively increased and the current flowing through the counter electrode was measured.

Ion release

The ion release test was performed by immersing the samples (treated and untreated) in 6 mL of conventional simulated body fluid (SBF, Table 1), at pH = 7.4, 37 °C, for 30 days. At day 5, the SBF was changed to avoid saturation of the medium.

The released Ni was measured by means of graphite furnace atomic absorption spectroscopy (GFAAS) (AAS Solar 989, Unicam, Germany) at 1 and 5 h and at 1, 2, 5 and 15 days. The results are mean values of three measurements.

Statistical analysis

The data were statistically analysed using *t*-Student tests, one-way ANOVA tables and Tukey's multiple comparison tests in order to evaluate statistically significant differences between the sample groups. The differences were considered significant when p-value <0.05. All statistical analyses were performed with Minitab™ software (Minitab release 13.0, Minitab Inc., USA).

Results and discussion

Figure 2 shows that the porous NiTi shape-memory alloys prepared for combustion possessed characteristics of a three-dimensionally intercommunicated structure that is permeable and open. In this study, the average pore size of porous NiTi (porosity: 62–65%) was between 250 and 360 μm. This size increased with porosity. Three orthogonal dimensions were observed with similar results, indicating an isotropic pore-growth structure. Micrographs of cross-sections confirm this by showing no preferred direction of pore growth or coalescence.

The pore-size parameters met the requirements for porous biomaterial used in cancellous bone implants [16, 17]. According to other authors, the configuration of open cellular material can be modelled as a connected network of rods forming open cells [18–20].

Table 1 Ion concentration of SBF and human blood plasma

	Concentration (mM)							
	Na^+	K^+	Mg^{2+}	Ca^{2+}	Cl^-	HCO^{3-}	HPO_4^{2-}	SO_4^{2-}
SBF	142.0	5.0	1.5	2.5	148.8	4.2	1.0	0.5
Human blood plasma	142.0	5.0	1.5	2.5	103.0	27.0	1.0	0.5

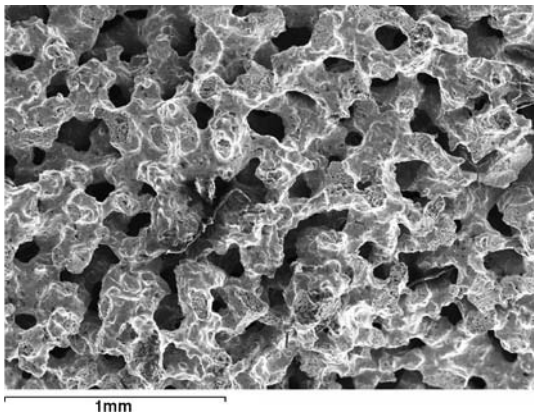

Fig. 2 SEM micrograph of the interconnected-porous NiTi foams

Surface chemical composition

Using XPS and argon sputtering, we detected a nearly 20-nm-thick layer that was practically Ni-free, followed by a progressive increase in Ni concentration in the treated samples (Fig. 3). The absence of Ni on the surface is essential to preventing the release of this ion, which produces an allergic reaction in a large percentage of the population.

The new heat treatment combines a very low surface Ni concentration with a thick protective oxide. This treatment is performed in a low oxygen pressure atmosphere and leads to specific Ti oxidation, as explained by Chan et al. [6]. We detected no Ni oxides with TiO_2, unlike with thermal treatments carried out at atmospheric pressure [6, 21, 22]. A low-Ni zone formed beneath the surface. Based on studies published in the literature, an oxidation pathway could to explain these results. According to Armitage et al. [22], at 400 °C, the oxide layer is predominantly formed by the inward diffusion of O ions inside the NiTi lattice. Because $\Delta G_{\text{formation (298 K)}}$ for TiO_2 and NiO are –212.6 kcal mol^{-1} and –50.6 kcal mol^{-1}, respectively [3, 14, 23], there is a preferential oxidation of Ti. Ni remains in its metallic state. The formation of stoichiometric TiO_2 is progressive and TiO_x ($x < 4$) may be present underneath [21] at the TiO_2–NiTi interface. Espinós et al. [24] showed that, under these conditions, Ni° interacts with Ti^{n+} ions ($n < 4$) and diffuses through TiO_x. Ni° disappears from the surface due to a migration in deeper layers.

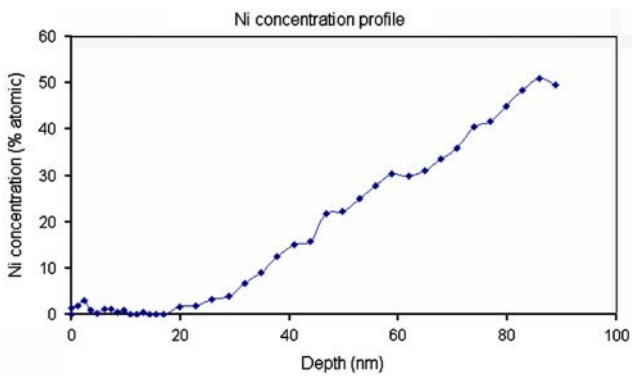

Fig. 3 Nickel concentration profile of oxidized samples

Phase-transformation temperatures

The results of the DSC measurements for untreated NiTi reveal an austenite transformation with a broad peak at 30 °C (A_s = 73 °C) and an enthalpy of ΔH = 2.3 J/g. The martensitic phase limits are found, respectively, at 69 °C (M_s) and 50 °C (M_f) with ΔH = 2.3 J/g. The samples remain in the martensite phase at body temperature.

The DSC measurements for the treated material show an austenite transformation with a broad peak at 26 °C (A_s = 78 °C) and an enthalpy of ΔH = 3.0 J/g. The martensite phase limits are found, respectively, at 70 °C (M_s) and 52 °C (M_f) with ΔH = 2.2 J/g. The treated NiTi foams also remain in the martensite phase at the body temperature.

Differential scanning calorimetry curves showed that phase-transformation temperatures M_s, M_f and A_f remained practically constant after the oxidation treatment (Table 2). However, A_s increased in the treated samples. (The material was supplied in martensitic structure.) This behaviour can be attributed to the increase in the oxygen content dissolved in the beta phase of NiTi. This oxygen produces an anchorage at the martensitic-beta phase interfaces, which acts as an obstacle to transformation (martensite → beta or austenitic phase). Consequently, further heating is necessary, which increases A_s. The enthalpy of the retransformation was therefore 3.1 J/g for the treated samples and 2.2 J/g for the untreated samples [25, 26].

A single peak appeared during the cooling cycle, indicating that the phase transformation from austenite to

Table 2 Phase-transformation temperatures

Material	A_s (°C)	A_f (°C)	ΔH (J/g)	M_s (°C)	M_f (°C)	ΔH (J/g)
Untreated	73	103	2.2	69	50	2.3
Treated	78	104	3.0	70	52	2.2

martensite occurred without the interposition of an R-phase. The transformation temperatures of Ni–Ti foams, A_f and M_s, are critical factors in their transformation behaviour, and the oxidation treatment does not affect these critical temperatures [27].

Compression tests

The compressive stress–strain curve of porous NiTi has three parts: (1) an apparent linear elastic phase, in which cell walls bend or are compressed elastically, (2) a stress yield phase of increasing slope, in which cells collapse by buckling and plastic-yielding, (3) a maximum-stress phase, followed by fracture failure. In the last phase, cell walls contact each other and are compressed. Pores may participate in the deformation process [20]. Table 3 shows the mechanical properties. These results show no statistically significant differences ($p < 0.005$) between the treated and untreated samples. Young's modulus, which is also important for the design of biomaterials for bone substitution, is very similar for porous NiTi and cancellous bone. This helps transfer the load from implant to bone, which minimizes the stress-shielding effect.

The stress–strain curve of cancellous bone in compression is very similar to that of NiTi foams. It also has three parts: a linear elastic phase, an apparent plateau of almost constant stress, and a final densification phase. However, as explained above, the mechanical properties of cancellous bone (except for Young's modulus) are very different from those of porous NiTi shape-memory alloys, especially in the second part of the curve. The small increase in stress with increased deformation in NiTi may be due to the orientation or coalescence of martensitic plates in the direction of the stress.

Corrosion behaviour

The free potential vs. Ag/AgCl reference electrode for treated and untreated porous NiTi samples were 165 mV and –250 mV, respectively (Fig. 4). This indicates that the oxidation treatment increases corrosion resistance.

The cyclic potential curves confirmed this behaviour. The pitting potential was slightly higher in the treated samples than in the untreated ones (Fig. 5).

The surface of the untreated NiTi contains titanium and nickel oxides, while treated NiTi contains only titanium oxide. Ni may dissolve more easily than Ni because its oxide is not as stable. Surface layers of Ni–Ti have irregular features characterized by lengthy island-like structures where selective dissolution of Ni may occur [29, 30].

The formation of thick and homogeneous stoichiometric TiO_2 on the surface of NiTi alloys improves the corrosion resistance of the material.

Ion release

This inert film of titanium oxide reduces the release of the metallic ion into the environment and acts as an obstacle to biodegradation. Figure 6 shows the release of ions. In both cases, the concentration of ions released into the medium initially increases very sharply and later reaches a saturation level [31–33].

This oxide is protective and reduces Ni release into the medium. Although the quantity of Ni ions released is well below 300–500 μg (the critical concentration for inducing allergy [33]), this quantity might be enough to induce long-term inflammatory responses or alter cell behaviour, even in untreated surfaces. Sun et al. [34] showed that metal ions can alter osteoblast behaviour even at subtoxic concentrations. Some studies have shown a significant decrease in alkaline phosphatase activity (ALP) and DNA synthesis with Ni ions. Other works have shown that Ni ions could be responsible for inducing the secretion of different cytokines involved in the inflammatory process. Wataha et al. [35] observed an increase in IL1β secretion by macrophages at Ni concentrations known to be released by NiTi dental materials. Another study [36] demonstrated that the quantity of IL1β secreted from monocytes due to

Table 3 Mechanical properties of the NiTi foams tested in compression

Material	E (GPa)	σ_0 (MPa)	σ_{max} (MPa)	ε (%)
Untreated NiTi	1.21 ± 0.31	101 ± 14	122 ± 29	22 ± 8
Treated NiTi	1.23 ± 0.37	103 ± 23	125 ± 26	21 ± 9
Cancellous bone [28]	1.08 ± 0.86	15 ± 8	25 ± 8	7 ± 3

E: Young's modulus, σ_0: yield stress, σ_{max}: maximum strength, ε: strain to fracture

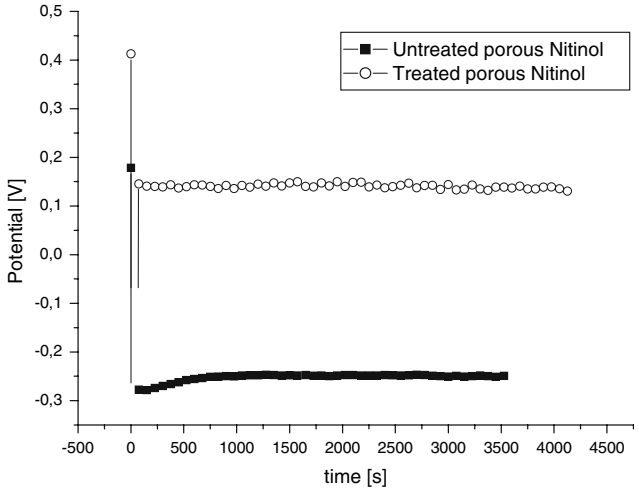

Fig. 4 Free potential curves

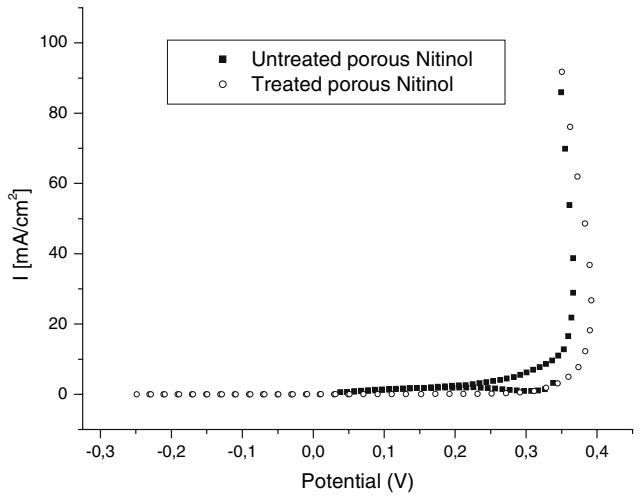

Fig. 5 Cyclic potentiodynamic curves

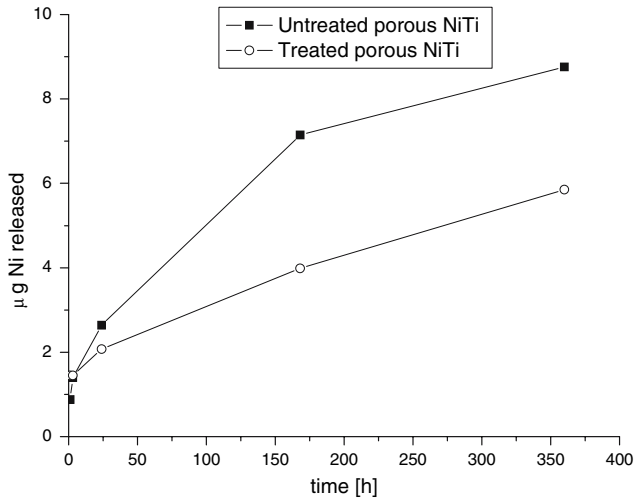

Fig. 6 Mass of Ni released in the simulated body fluid over time

the release of Ni ions (7.2 µg/mL) was large enough to indirectly induce the secretion of ICAM1 (intracellular adhesion molecules involved in the recruitment of other inflammatory cells) on endothelial cells. Finally, Cederbrant et al. [37] showed that a quantity of Ni even as small as 1.2 µg/mL could induce an increase in the proliferation of lymphocytes and the secretion of IL10 in subjects allergic to Ni. Thus, the results obtained for oxidized surfaces may help improve the long-term biocompatibility properties of materials and reduce sensitization to Ni and allergies.

The improved corrosion resistance of treated NiTi is due to the stable titanium oxide on the surface. Moreover, oxides with a high dielectric constant have been hypothesized to cause less protein denaturation than surfaces with a low dielectric constant. Ti, which forms a stable oxide with a high dielectric constant and exhibits intimate bonding to bone, is consistent with this suggestion [38].

Conclusions

The oxidation treatment for foams of Ni–Ti alloys effectively and reliably reduces the amount of Ni released into physiological media. This is achieved by forming a Ni-free oxide layer on the surface. Furthermore, the treatment improves the corrosion resistance of the alloy and hardly changes the phase-transformation temperatures. Further studies must be carried out to ensure the biological effectiveness and safety of the treatment.

Acknowledgements The authors would like to thank Dr. Jose M. Manero for his help with scanning electron microscope imaging and sample preparation and CICYT (MAT2003-08165 and MAT2005-07244) for its financial support.

References

1. J. C. WATAHA, N. L. O'DELL, B. B. SINGH, M. GHAZI, G. M. WHITFORD and P. E. LOCKWOOD, *J. Biomed. Mater. Res. B* **58** (2001) 537
2. L. PELTONEN, *Contact Derm.* **5** (1979) 27
3. C. L. DUNLAP, S. K. VINCENT and B. F. BARKER, *JADA* **11** (1989) 449
4. M. CEJNA, R. VIRMANI, R. JONES, H. BERGMEISTER, C. LOEWE, M. SCHRODER, M. GRGURIN and J. LAMMER, *J. Vasc. Interv. Radiol.* **12** (2001) 351
5. S. A. SHABALOVSKAYA and J. W. ANDEREGG, *J. Vasc. Sci. Technol. A* **13** (1995) 2624
6. C. M. CHAN, S. TRIGWELL and T. DUERIG, *Surf. Interface Anal.* **15** (1990) 349
7. R. HERNANDEZ, S. POLIZU, S. TURENNE and L'H. YAHIA, *Biomed. Mater. Eng.* **12** (2002) 37
8. R. A. AYERS, T. A. BATEMAN and S. J. SIMSKE, *Shape Memory Implants* (London: Springer Verlag, 2000), p. 126
9. V. I. HIN, V. E. GJUNTER, S. A. SHABALOVSKAYA and R. L. C. SACHDEVA, *Mater. Character.* **32** (1994) 179

10. M. M. VILA, M. P. GINEBRA, F. J. GIL and J. A. PLANELL, *J. Biomed. Mater. Res.* **48** (1999) 121
11. M. M. VILA, M. P. GINEBRA, F. J. GIL and J. A. PLANELL, *J. Biomed. Mater. Res.* **48** (1999) 128
12. A. MICHIARDI, C. APARICIO, J. A. PLANELL and F. J. GIL, *J. Biomed. Mater. Res. B* **77B** (2006) 249
13. A. MICHIARDI, C. APARICIO, J. A. PLANELL and F. J. GIL, Spanish Patent no. 2251312 (2006)
14. S. TRIGWELL, R. D. HAYDEN, K. F. NELSON and G. SELVADURAY, *Surf. Interface Anal.* **26** (1998) 483
15. S. A. SHABALOVSKAYA, J. ANDEREGG, F. LAAB, P. A. THIEL and G. RONDELLI, *J. Biomed. Mater. Res. B* **65** (2003) 193
16. Y. H. LI, L. J. RONG and Y. Y. LI, *J. Alloys Compd.* **325** (2001) 259
17. V. H. ITIN, V. E. GJUNTER and S. A. SHABALOVSKAYA, *Mater. Character.* **32** (1994) 179
18. L. J. GIBSON, *J. Biomech.* **18** (1995) 317
19. M. F. ASHBY, *Metall. Trans. A* **26A** (1983) 1755
20. Y. H. LI, L. J. RONG and Y. Y. LI, *J. Alloys Compd.* **345** (2002) 271
21. G. S. FIRSTOV, R. G. VITCHEV, H. KUMAR, B. BLANPAIN and J. VAN HUMBEEK, *Biomaterials* **23** (2002) 4863
22. D. A. ARMITAGE and D. M. GRANT, *Mater. Sci. Eng. A* **349** (2003) 89
23. S. M. GREEN, D. M. GRANT and J. V. WOOD, *Mater. Sci. Eng. A* **224** (1997) 21
24. J. P. ESPINOS, A. FERNANDEZ and A. R. GONZALEZ-ELIPE, *Surf. Sci.* **295** (1993) 402
25. F. J. GIL, J. M. MANERO and J. A. PLANELL, *J. Mater. Sci.: Mater. Med.* **7** (1996) 403
26. F. J. GIL, C. LIBENSON and J. A. PLANELL, *J. Mater. Sci.: Mater. Med.* **4** (1993) 281
27. T. SAWADA, H. TOBUSHI, K. KIMURA, T. HATTORI and K. TAMAKA, *Trans. Jpn. Soc. Mech. Eng. Ser. A* **3** (1993) 959
28. S. J. KAPLAN, W. C. HAYES and J. L. STONE, *J. Biomech.* **18** (1985) 723
29. F. J. GIL, E. SOLANO, J. PENA, E. ENGEL, A. MENDOZA and J. A. PLANELL, *J. Mater. Sci.: Mater. Med.* **15** (2004) 1181
30. J. RYHANEN, E. NIEMI, W. SERLO, E. NIAMELA, P. SANDVICK, H. PERNU and T. SALO, *J. Biomed. Mater. Res.* **35** (1997) 451
31. F. J. GIL, E. SOLANO, J. PENA and A. MENDOZA, *J. Appl. Biomater. BiomeCH.* **2** (2004) 151
32. F. J. GIL, E. SOLANO, A. CAMPOS, F. BOCCIO, I. SAEZ, M. V. ALFONSO and J. A. PLANELL, *Bio-Med. Mater. Eng.* **8** (1998) 335
33. H. H. HUANG, Y. H. CHIU, T. H. LEE, S. C. WU, H. W. YANG, K. H. SU and C. C. HSU, *Biomaterials* **24** (2003) 3585
34. Z. L. SUN, J. C. WATAHA and C. T. HANKS, *J. Biomed. Mater. Res.* **34** (1997) 29
35. J. C. WATAHA, S. RATANASATHIENZ, C. T. HANKS and Z. SUN, *Dental Mater.* **12** (1996) 322
36. J. C. WATAHA, P. E. LOCKWOOD, M. MAREK and M. GHAZI, *J. Biomed. Mater. Res.* **45** (1999) 251
37. K. CEDERBRANT, C. ANDERSSON, T. ANDERSSON, M. MARCUSSON-STAHL and P. HULTMAN, *Int. Arch. Allergy Immunol.* **132** (2003) 373
38. T. ALBREKTSSON, P.-I. BRANEMARK, H. A. HANSSON, B. KASEMO, K. LARSSON, I. LUNDSTROM, D. H. MCQUEEN and R. SKALAK, *Ann. Biomed. Eng.* **11** (1983) 1